Journal of Materials Science: Materials in Electronics (2018) 29:17689–17694
https://doi.org/10.1007/s10854-018-9874-6

Microstructure and dielectric properties of $BaTiO_3$–$(Bi_{0.5}Na_{0.5})TiO_3$–$NiNb_2O_6$ ceramics

Mi Xiao[1] · Hongrui Sun[1] · Yanshuang Wei[1] · Lei Li[1] · Ping Zhang[1]

Received: 22 April 2018 / Accepted: 14 August 2018 / Published online: 27 August 2018

Abstract
$0.9BaTiO_3$–$0.1(Bi_{0.5}Na_{0.5})TiO_3$–x mol% $NiNb_2O_6$ (x = 0, 0.5, 1.0, 1.5, 2.0, 2.5) ceramics were prepared through traditional solid-state reaction method. The effects of $NiNb_2O_6$ doping on the dielectric properties and the microstructure of ceramics were investigated systematically. The results showed that the grain size of the ceramics decreased with the increase of $NiNb_2O_6$ doping amount. $Ba_{11}(Ni,Ti)_{28}O_{66+x}$ and Nb_2O_5 were detected in the X-ray diffractions patterns. The Curie point T_c increased slightly with the increase of $NiNb_2O_6$ doping amount. It was interesting to find that the dielectric constant at low temperature of the ceramics first increased and then decreased with the increase of $NiNb_2O_6$ concentration. Dielectric temperature stability of $0.9BaTiO_3$–$0.1(Bi_{0.5}Na_{0.5})TiO_3$ ceramics greatly depended on $NiNb_2O_6$ content. The optimum dielectric properties meeting the X9R specification were obtained in the composition of $0.9BaTiO_3$–$0.1(Bi_{0.5}Na_{0.5})TiO_3$ with 1.5 mol% $NiNb_2O_6$ sintered at 1200 °C, $\varepsilon_r = 1652$ and $\tan\delta = 1.8\%$ at room temperature.

1 Introduction

Recent developments in modern electronic devices have brought new demands for multilayer ceramic capacitors (MLCCs) with higher performances. However, one of the major problems of MLCCs is to raise the upper limit of operating temperature under the premise of keeping high temperature-stable dielectric constant and high reliability [1–3]. Although X8R (− 55 to 150 °C, $\Delta C/C_{25°C} \leq \pm 15\%$) MLCCs have been widely studied and reported in many research groups [4–6], it is necessary to exploit new ceramics systems which satisfy EIA-X9R specification (− 55 to 200 °C, $\Delta C/C_{25°C} \leq \pm 15\%$) due to the emergence of many new applications working in the environment with broadened high temperature range [7].

The pure $BaTiO_3$ (BT) ceramic has a sharp phase transition peak at Curie temperature (T_c), which seriously deteriorates temperature stability. To improve the temperature stability, there are mainly two methods: (1) Preparing a solid solution with higher Curie temperature by doping an effective Curie temperature shifter in $BaTiO_3$, such as $(Bi_{0.5}Na_{0.5})TiO_3$ (BNT) [8, 9] or $(K_{0.5}Na_{0.5})NbO_3$ [10, 11]. For example, the T_c of the solid solution 0.9BT–0.1BNT is above 160 °C [9], much higher than that of pure BT (125 °C); (2) Forming a fine-grained core–shell structure in the BT-based ceramics [12–14]. The dielectric temperature characteristics of the ceramics with a core–shell structure could be evaluated using the Lichtenecker formula [15]:

$$\log \varepsilon = V_c \log \varepsilon_c + V_s \log \varepsilon_s \quad (1)$$

where V_c, V_s and ε_c, ε_s are the volume fraction and the relative dielectric constant of the ceramics in core and shell, respectively. At room temperature, the core part is tetragonal ferroelectric phase and the shell part is pseudo-cubic paraelectric phase. By the way, Curie temperature is the temperature at which there will be a phase transition from ferroelectric to paraelectric. The overall dielectric exhibits an insensitive dielectric response to temperature due to the diffuse phase transition caused by the core–shell structure [16]. Therefore the core–shell structure can help to improve the temperature stability of the dielectric properties.

Considering those two methods mentioned above, many researchers pay more attentions to the core–shell structure in 0.9BT–0.1BNT system. Because of the low diffusion velocity in BT, Nb_2O_5 is the most common dopant used

✉ Mi Xiao
xiaomi@tju.edu.cn

✉ Ping Zhang
zptai@163.com

[1] School of Electrical and Information Engineering & Key Laboratory of Advanced Ceramics and Machining Technology of Ministry of Education, Tianjin University, Tianjin 300072, People's Republic of China

in 0.9BT–0.1BNT system to form the core–shell structure [17–20]. When Nb_2O_5 is added, Nb^{5+} will substitute for Ti^{4+}, acting as a donor, and the substitution process will unexpectedly increase the concentration of defects. The co-doping of donor and acceptor has been taken to solve this problem. But another problem is that most kinds of dopants would decrease T_c. For example, it was reported that the substitution of Ni^{2+} for Ti^{4+} caused a decrease of T_c in 0.9BT–0.1BNT–Nb_2O_5 ceramics [21]. Meanwhile, the addition of Ni^{2+} can be achieved by the doping of $NiNb_2O_6$. Previous research has established that T_c of BT–$CaZrO_3$ ceramics can be promoted slightly with the increase of $NiNb_2O_6$ doping amount, and the 1.5 wt%-doped sample showed the optimal dielectric performance meeting the X8R specification [22]. However, the relative study about BT-based ceramics doped with $NiNb_2O_6$ is still insufficient.

In this paper, 0.9BT–0.1BNT–x mol% $NiNb_2O_6$ ceramics were prepared through solid-state reaction method and the effects of $NiNb_2O_6$ on the microstructure and dielectric properties of 0.9BT–0.1BNT ceramics were studied.

2 Experimental procedure

BT–BNT–$NiNb_2O_6$ ceramic samples were prepared through traditional solid-state reaction method. $NiNb_2O_6$ and BNT powders were pre-synthesized using reagent grade NiO, Nb_2O_5, Na_2CO_3, Bi_2O_3, and TiO_2 as raw materials, and calcined at 1000 °C for 2 h and 900 °C for 2 h [19, 23], respectively. $BaTiO_3$ powder with an average size of 300 nm was mixed with the obtained BNT at a molar ratio of 9:1, then calcined at 1050 °C for 8 h to obtain the 0.9BT–0.1BNT solid solution [18]. Subsequently, various amounts of $NiNb_2O_6$ (0, 1.0, 1.5, 2.0, 2.5 mol%) were added into the solid solution of 0.9BT–0.1BNT, and then ball-milled with the deionized water for 6 h. After dried, the powders were pressed into discs with 15 mm in diameter and 1 mm in height under the pressure of 4 MPa [22]. These discs were sintered at 1200–1250 °C for 3 h in air with a heating rate of 5 °C/min [18, 24].

The phase structures of the specimens were detected by the X-ray diffraction (XRD) analysis (XRD, Rigaku D/max 2550 PC, Tokyo, Japan, with Cu Kα radiation generated at 40 kV and 40 mA). According to the work of the predecessors [25–28], XRD patterns of samples were obtained in Bragg–Brentano (θ–2θ) geometry. The microstructures of ceramics were observed by scanning electron microscopy (SEM, MERLIN Compact, Germany). The average grain sizes were analyzed using the NanoMeasurer software. For the dielectric properties measurements, silver electrode paste was coated on the opposing surfaces of the sintered samples and sintered at 850 °C for 30 min for deoxidization. The dielectric properties were measured from − 55 to 200 °C (at a heating rate of 3 °C/min) using LCR meter (HP4278A, HP, USA) at 1 kHz and oscillation level of 1.0 V.

3 Results and discussions

3.1 XRD analysis

Figure 1 shows the XRD patterns of the ceramic samples with different amount of $NiNb_2O_6$. The desired perovskite phase was observed in all samples, and two kinds of secondary phases including $Ba_{11}(Ni,Ti)_{28}O_{66+x}$ and Nb_2O_5 were detected with the increase of $NiNb_2O_6$ doping amount. $Ba_{11}(Ni,Ti)_{28}O_{66+x}$ appeared when the $NiNb_2O_6$ doping amount was greater than 2.0 mol%, and the relative concentration increased with the increase of $NiNb_2O_6$ addition. It is reported that the valence of Ni in $Ba_{11}(Ni,Ti)_{28}O_{66+x}$ is +3 [21], which indicates the transformation of some Ni^{2+} to Ni^{3+} during the sintering of the ceramics. The appearance of Ni^{3+} suppress the solubility of Nb^{5+} in the lattice, therefore we can find the phase of Nb_2O_5 in the XRD patterns when x = 2.5. For BT, there are two adjacent diffraction peaks around 46°: (002) and (200). As it can be seen from the inset of Fig. 1, the two peaks (002) and (200) are split in the un-doped 0.9BT–0.1BNT ceramic. They gradually merged together by increasing the concentration of $NiNb_2O_6$ to 1.5 mol%. However, slightly split was found with the further increase of the concentration. In addition, it is found that the diffraction peaks shift towards lower degree when x was changed from 0 to 1.5. However, the shift cannot be observed when x ≥ 2.0. These results were attributed to the difference in radius of doping ions and substituted ions.

The extrapolated ionic radius of Ni^{3+} (0.56 Å) is smaller than that of Ti^{4+} (0.605 Å), and the radii of Ni^{2+} (0.69 Å)

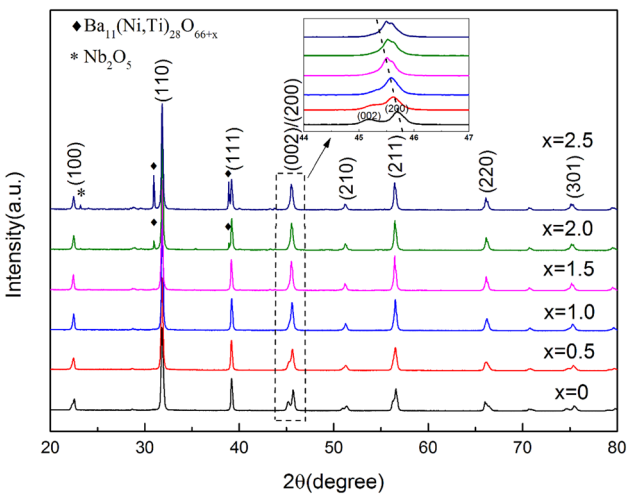

Fig. 1 XRD patterns of samples with various amounts of $NiNb_2O_6$

and Nb^{5+} (0.64 Å) are bigger than that of Ti^{4+}. When the doping amount of $NiNb_2O_6$ is less than 2.0 mol%, with the increase of $NiNb_2O_6$ substitution, the diffraction peaks shift towards lower degree, which indicated that small amount of $NiNb_2O_6$ doping could increase the unit cell volume because of the bigger radii of Ni^{2+} and Nb^{5+} than that of Ti^{4+}. The substitution also suppressed the polarization of Ti–O octahedral, as a result, the lattice gradually changed from tetragonal to pseudo-cubic, and (002) and (200) gradually merged together. When the doping amount of $NiNb_2O_6$ is greater than 2.0 mol%, since there isn't any obvious shift of the diffraction peaks with the increase of $NiNb_2O_6$ doping amount, the substitution for Ti^{4+} must include some smaller ions, which should be Ni^{3+}. The substitution of Ni^{3+} for Ti^{4+} will lead to a decrease in unit cell volume and strengthening of polarization, which can offset the influence of Ni^{2+} and Nb^{5+}, thus the shift of diffraction peaks was not obvious, and the lattice gradually changed from pseudo-cubic to tetragonal.

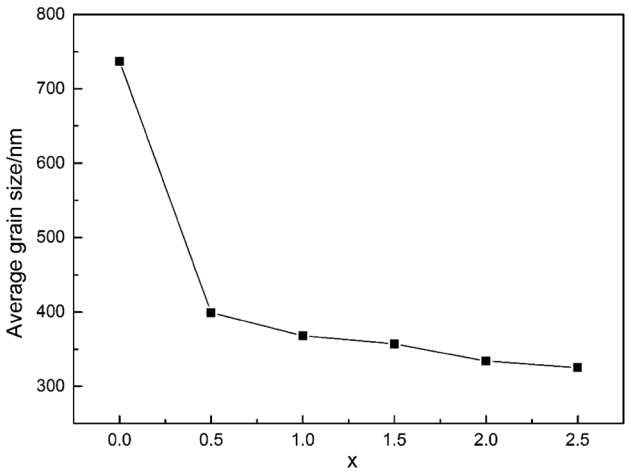

Fig. 3 Average grain sizes of samples with various amounts of $NiNb_2O_6$

3.2 SEM analysis

Surface morphologies of the 0.9BT–0.1BNT–x mol% $NiNb_2O_6$ samples are shown in Fig. 2. From Fig. 2 we can see that all the samples are highly densified. Moreover, the coexistence of smaller grains and larger grains is confirmed, and the number of smaller grains increased with the doping amount of $NiNb_2O_6$. Figure 3 shows the effect of $NiNb_2O_6$ content on the average grain size of ceramics, from which we can know that the average grain sizes of ceramics doped with $NiNb_2O_6$ are much smaller than that of un-doped BT–BNT ceramic. However, there are some flake-like grains formed when $x \geq 2.0$. Here we just show the flake-like grains in 0.9BT–0.1BNT–2.5 mol% $NiNb_2O_6$ sample in Fig. 4a to observe the appearance of them. As shown in Fig. 4b, the EDS result of the flake-like grain indicated that it is composed of four elements, Ba, Ti, Ni and O, which corresponds to the $Ba_{11}(Ni,Ti)_{28}O_{66+x}$ phase in XRD patterns.

3.3 Dielectric properties

The temperature dependences of dielectric properties of 0.9BT–0.1BNT–x mol% $NiNb_2O_6$ ceramics (x = 0.5, 1.0,

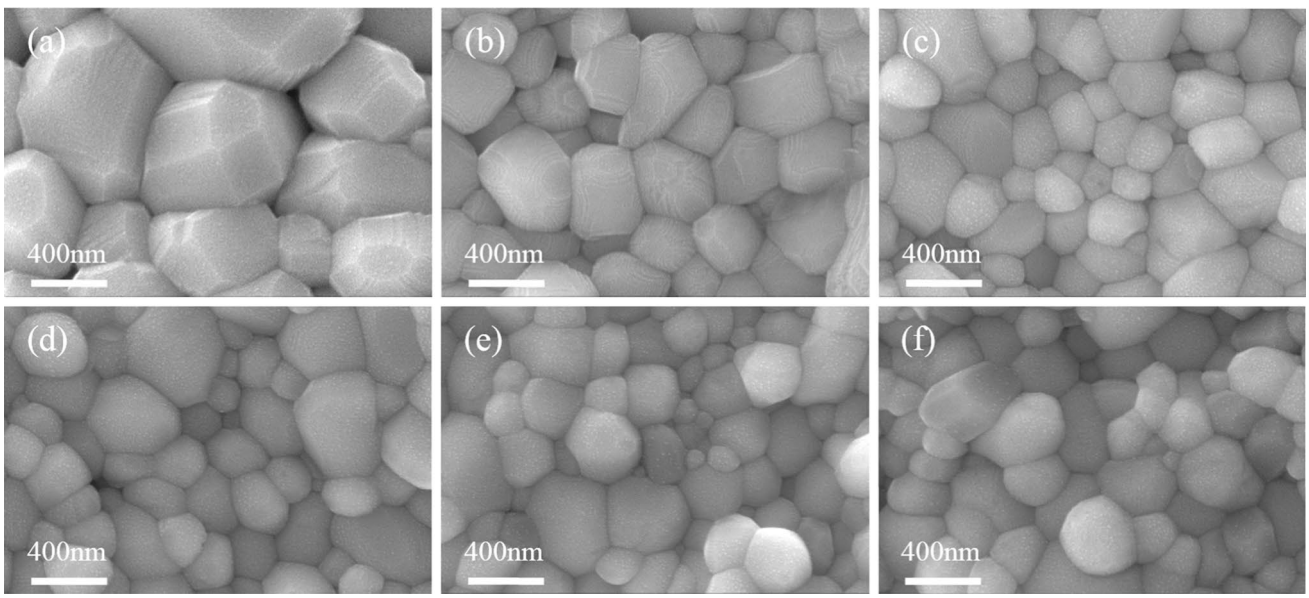

Fig. 2 SEM of 0.9BT–0.1BNT–x mol% $NiNb_2O_6$ ceramics: **a** x = 0, **b** x = 0.5, **c** x = 1.0, **d** x = 1.5, **e** x = 2.0, **f** x = 2.5

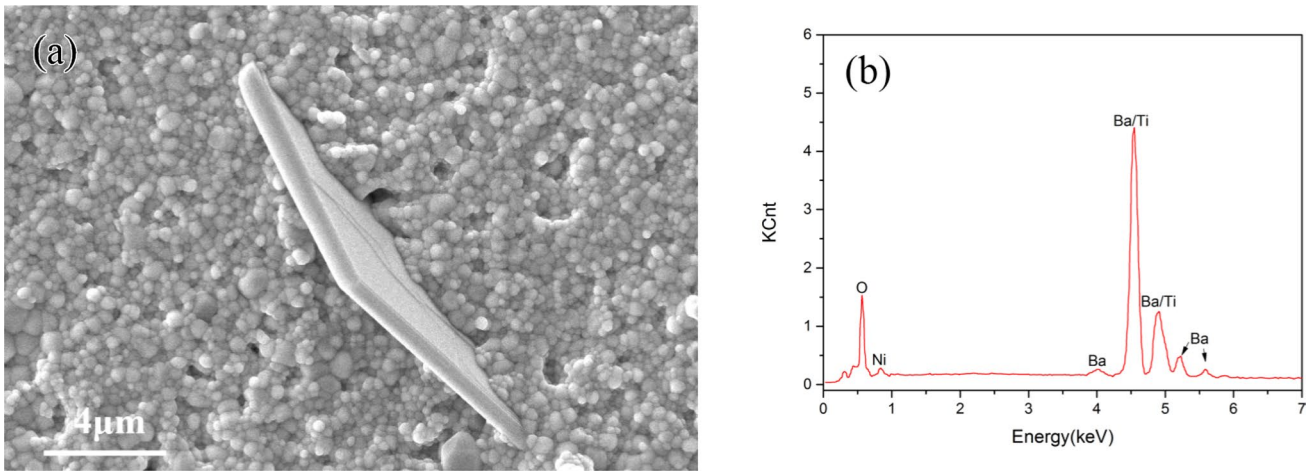

Fig. 4 **a** SEM images of 0.9BT–0.1BNT–2.5 mol% $NiNb_2O_6$ ceramic. **b** EDS result of the flake-like grain in 0.9BT–0.1BNT–2.5 mol% $NiNb_2O_6$ ceramic

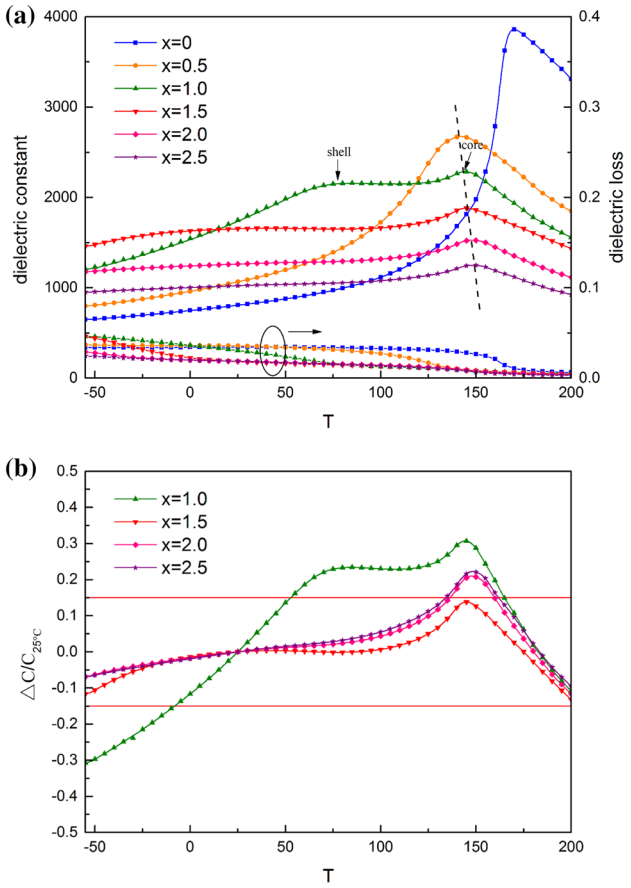

Fig. 5 Temperature dependence of **a** dielectric constant and dielectric loss; **b** capacitance change (TCC = $\Delta C/C_{25°C}$) at 1 kHz for $NiNb_2O_6$ doped BT–BNT ceramic samples

1.5, 2.0, 2.5) are displayed in Fig. 5, from which we can see that with the increase of $NiNb_2O_6$ content, two dielectric constant peaks appeared, as marked by the two arrows. The high temperature peak and the low temperature peak are corresponding to the core phase and the shell phase, respectively, indicating the existence of core–shell structure [29]. However, the low temperature peak was hard to be observed when the doping level was 0.5 mol%, 2 mol% and 2.5 mol%. When doped level was 0.5 mol%, the $NiNb_2O_6$ doping amount is too low so that the volume fraction of shell region is very small. Therefore the low temperature peak is hard to be observed. With the increase of $NiNb_2O_6$ content, the two peaks were broadened due to the diffuse phase transition behaviors, and the peak of shell region is gradually obscured by the low temperature tail of the Curie peak. So it is hard to be observed either when x is greater than 1.5. In addition, the dielectric constant peak of core phase T_c shifted towards the higher temperature with the increase of doping amount of $NiNb_2O_6$, just as shown as dash line in Fig. 5. Given that the ceramics doped with 0 and 0.5 mol% $NiNb_2O_6$ do not meet the requirements of X9R specification, $\Delta C/C_{25°C}$ of these two samples are not shown in Fig. 5b for clarity. Table 1 gives the dielectric properties of 0.9BT–0.1BNT–x mol% $NiNb_2O_6$ ceramics, from which it can be known that all the dielectric loss detected are below 5%, and the temperature dependence of the samples changed with $NiNb_2O_6$ doping amount accordingly. It should be noted that 0.9BT–0.1BNT–1.5 mol% $NiNb_2O_6$ sample presents the most flattened temperature dependency, satisfying the X9R specification, and the dielectric properties are $\varepsilon_r = 1652$, $\tan\delta = 1.8\%$.

From Fig. 5 we can see that for the 0.9BT–0.1BNT–x mol% $NiNb_2O_6$ samples, the ε_r–T curves changes in a clockwise direction with the increase of $NiNb_2O_6$ doping amount

Table 1 Dielectric properties of 0.9BT–0.1BNT–x mol% $NiNb_2O_6$ ceramics at 1 kHz

Samples	ε_r (25 °C)	tanδ (%) (25 °C)	T_c (°C)	$\Delta C/C_{25°C}$ (%)		
				− 55 °C	150 °C	200 °C
0.9BT–0.1BNT	807	3.4	170.0	− 19.8	144.7	309.8
0.9BT–0.1BNT–0.5 mol% $NiNb_2O_6$	1066	3.6	142.1	− 25.2	145.6	73.4
0.9BT–0.1BNT–1.0 mol% $NiNb_2O_6$	1748	3.1	144.0	− 30.8	28.8	− 10.9
0.9BT–0.1BNT–1.5 mol% $NiNb_2O_6$	1652	1.8	144.9	− 11.7	12.6	− 13.3
0.9BT–0.1BNT–2.0 mol% $NiNb_2O_6$	1263	1.9	147.7	− 6.8	20.7	− 11.7
0.9BT–0.1BNT–2.5 mol% $NiNb_2O_6$	1022	1.9	148.6	− 6.9	22.1	− 9.5

up to 1.5 mol%. In other words, dielectric constant decreases at high temperature end, and increases at low temperature end. This is due to the decrease of volume ratio of core and the increase of volume ratio of shell in the grain. However, the curves show an overall decline with the further increase of $NiNb_2O_6$ amount, which is related to the grain size and second phase. It is apparent from Fig. 3 that the average grain size decreased with the increase of $NiNb_2O_6$ content, which is caused by pinning effects [30]. The shell "$NiNb_2O_6$-doped BT–BNT" acted as diffusion barrier and prevented BT–BNT core from grain boundary diffusion/migration and grain growth. The decreased grain size caused the increase of the grain boundary area per unit volume. Actually, the width of grain boundary is not negligible, and it could be considered fixed [31]. Therefore the volume ratio of the grain boundary in the ceramics increased with the increase of $NiNb_2O_6$ content. That is to say, a great deal of non-ferroelectric phase is introduced in ferroelectric ceramics with the increase of $NiNb_2O_6$ content, which reduces the dielectric constant of the entire ceramic system accordingly. The formation of second phase also shows impact on the dielectric properties. Since $Ba_{11}(Ni,Ti)_{28}O_{66+x}$ has similar synthesis condition as $Ba_{11}(Fe,Ti)_{28}O_{66+x}$, which has a rather low dielectric constant (< 100) and dielectric loss [32], it is reasonable $Ba_{11}(Ni,Ti)_{28}O_{66+x}$ has a low dielectric constant too. The combined effects of grain size and $Ba_{11}(Ni,Ti)_{28}O_{66+x}$ result in the decrease of dielectric constant when x is greater than or equal to 2.0.

Compared with the pure 0.9BT–0.1BNT, the T_c of the 0.9BT–0.1BNT–x mol% $NiNb_2O_6$ ceramics decreased. However, the T_c show an increasing behavior with the increase of $NiNb_2O_6$ content. There are three influence factors on T_c [33]: (1) the average ionic radium, here we just discuss $R_{B\text{-site}}$; (2) the statistical variance in the distribution of the radii σ^2, which can be used to describe the local strain field. $R_{B\text{-site}}$ and σ^2 can reflect the influence of lattice mismatch; (3) electrovalence mismatch between the doped ions and the matrix ions, which can reflect the local electric field. However, this mechanism is just applicable when the ion could be considered spherical [34]. The electrovalence mismatch and larger $R_{B\text{-site}}$ will lead to a drop of T_c, while larger σ^2 shows opposite effect. Electrovalence mismatch such as Ni^{2+} substituting for Ti^{4+} may introduce oxygen vacancies, which will increase the phase stability of cubic phase [35]. For BT-based ceramics, with the increase of concentration of doping, the $R_{B\text{-site}}$, σ^2, and electrovalence mismatch have been changed, which leads to the change of local strain field and local electric field. Therefore the diffuse phase transition behavior was affected, resulting in the change of the T_c.

When $x \leq 1.5$, Ni^{2+} and Nb^{5+} cations diffuse into the crystal lattice in the form of $(Ni_{1/3}{}^{2+}Nb_{2/3}{}^{5+})^{4+}$ with an effective radius of 0.66 Å which is larger than that of Ti^{4+}, and a valence of +4 which is identical to Ti^{4+}. In this condition, electrovalence mismatch does not exist, and $R_{B\text{-site}}$ and σ^2 both increase with the doping amount of $NiNb_2O_6$. With the supporting of the theory mentioned above, the change of T_c reveals that the absence of electrovalence mismatch and the larger σ^2 show more impact than $R_{B\text{-site}}$ and result in the increase of T_c. When x is greater than 2.0, the presence of Ni^{3+} is confirmed according to the former analysis, and the shift of the diffraction peaks is little. If Ni^{3+} and Nb^{5+} still diffuse into the crystal lattice according to the molar ratio of 1:2, the diffraction peaks should have shifted towards lower degree because the effective radius of $(Ni_{1/3}{}^{3+}Nb_{2/3}{}^{5+})^{13/3+}$ (0.613 Å) is larger than that of Ti^{4+}, which is not consistent with the fact. A possible explanation for this might be that Ni^{3+} and part of Nb^{5+} diffuse into the crystal lattice in the form of $(Ni_{1/2}{}^{3+}Nb_{1/2}{}^{5+})^{4+}$. The rest of Nb^{5+} appears in the form of Nb_2O_5, which has been proved by XRD in Fig. 1. $(Ni_{1/2}{}^{3+}Nb_{1/2}{}^{5+})^{4+}$ has an effective radius of 0.60 Å, just a little smaller than that of Ti^{4+}, and an identical valence to Ti^{4+}, so that the electrovalence mismatch is absent. $R_{B\text{-site}}$ decreased with the increases of $(Ni_{1/2}{}^{3+}Nb_{1/2}{}^{5+})^{4+}$ content, while σ^2 has little change. Therefore the substitution of $(Ni_{1/2}{}^{3+}Nb_{1/2}{}^{5+})^{4+}$ for Ti^{4+} made the T_c have a potential of further increase due to the absence of electrovalence mismatch and the smaller $R_{B\text{-site}}$. The collective effect of $(Ni_{1/3}{}^{2+}Nb_{2/3}{}^{5+})^{4+}$ and $(Ni_{1/2}{}^{3+}Nb_{1/2}{}^{5+})^{4+}$ on the ceramics results in the increase of T_c.

The Nb^{5+} as well as Ni^{2+} substituting for Ti^{4+} in 0.9BT–0.1BNT system leads to the monotonous reduction of T_c, but the doping of $NiNb_2O_6$ can promote T_c. This may suggest that we can use ion combinations with the same

valence and similar radius to Ti^{4+} to improve the T_c of BT-based ceramics.

4 Conclusion

The effects of $NiNb_2O_6$ content on microstructures and dielectric properties of 0.9BT–0.1BNT ceramics were studied in this paper. The results show that the doping of $NiNb_2O_6$ can suppress the grain growth. In spite of the facts that T_c of the doped samples are lower than that of un-doped 0.9BT–0.1BNT ceramic, T_c shows an increasing behavior with the increase of $NiNb_2O_6$ content. Dielectric constant at low temperature first increased and then decreased. The change of dielectric constant can be related to the cooperating influence of core–shell structure and grain size. And the increase of T_c can be explained by the change of $R_{B\text{-site}}$, σ^2 and electrovalence mismatch, which suggested a possible method to use proper ionic combinations to increase T_c. 1.5 mol% $NiNb_2O_6$-doped specimen met X9R specifications and exhibited excellent dielectric properties with a dielectric constant of 1652 and a dielectric loss of 1.8% at room temperature.

Acknowledgements This work was supported by the National Natural Science Foundation of China (Grant No. 61671323).

References

1. C. Groh, K. Kobayashi, H. Shimizu, Y. Doshida, Y. Mizuno, E.A. Patterson, J. Rödel, J. Am. Ceram. Soc. **99**(6), 2040–2046 (2016)
2. S. Wang, H. He, H. Su, J. Mater. Sci.: Mater. Electron. **23**(10), 1875–1880 (2012)
3. Z. Liu, H. Fan, S. Lei, X. Ren, C. Long, J. Eur. Ceram. Soc. **37**(1), 115–122 (2017)
4. S. Wang, H. He, H. Su, J. Mater. Sci.: Mater. Electron. **24**(7), 2385–2389 (2013)
5. L. Li, Y. Liu, M. Wang, N. Zhang, J. Chen, J. Mater. Sci.: Mater. Electron. **25**(10), 4252–4258 (2014)
6. X. Huang, H. Liu, H. Hao, Z. Wang, W. Hu, Q. Xu, J. Mater. Sci.: Mater. Electron. **26**(5), 3215–3222 (2015)
7. X. Huang, W. Zhang, J. Xie, Q. Xu, L. Zhang, J. Mater. Sci.: Mater. Electron. **28**(5), 4204–4210 (2017)
8. Z. Shen, X. Wang, L. Li, J. Mater. Sci.: Mater. Electron. **28**(4), 3768–3773 (2017)
9. G. Yao, X. Wang, Y. Wu, L. Li, J. Am. Ceram. Soc. **95**(2), 614–618 (2012)
10. Z. Hu, B. Cui, M. Li, L. Li, J. Mater. Sci.: Mater. Electron. **24**(10), 3850–3855 (2013)
11. Z. Hu, B. Cui, S. Jing, Y. Wang, Mater. Lett. **113**, 167–169 (2013)
12. T. Wang, H. Hao, M. Liu, D. Zhou, Z. Yao, M. Cao, H. Liu, J. Am. Ceram. Soc. **98**(3), 690–693 (2015)
13. M. Liu, H. Hao, W. Chen, D. Zhou, M. Appiah, B. Liu, Z. Zhang, Ceram. Int. **42**(1), 379–387 (2016)
14. R. Ma, B. Cui, M. Shangguan, S. Wang, Y. Wang, Z. Chang, Y. Wang, J. Alloys Compd. **690**, 438–445 (2017)
15. D. Hennings, G. Rosenstein, J. Am. Ceram. Soc. **67**(4), 249–254 (1984)
16. R. Farhi, M. El Marssi, A. Simon, J. Ravez, Eur. Phys. J. B **18**(4), 605–610 (2000)
17. Z.B. Shen, X.H. Wang, D.S. Song, L.T. Li, Adv. Appl. Ceram. **115**(7), 435–442 (2016)
18. G. Yao, X. Wang, Y. Zhang, Z. Shen, L. Li, J. Am. Ceram. Soc. **95**(11), 3525–3531 (2012)
19. Y. Zhang, S. Gao, B. Zhang, J. Mater. Sci.: Mater. Electron. **26**(5), 2709–2712 (2015)
20. Y. Sun, H. Liu, H. Hao, L. Zhang, S. Zhang, Ceram. Int. **41**(1), 931–939 (2015)
21. Y. Sun, H. Liu, H. Hao, Z. Song, S. Zhang, J. Am. Ceram. Soc. **98**(5), 1574–1579 (2015)
22. L. Li, J. Yu, N. Zhang, J. Ye, J. Mater. Sci.: Mater. Electron. **26**(12), 9522–9528 (2015)
23. C.Y. You, Y.C. Zhang, J. Mater. Sci.: Mater. Electron. **27**(6), 6606–6613 (2016)
24. S.F. Wang, Y.F. Hsu, Y.W. Hung, Y.X. Liu, Appl. Sci. **5**(4), 1221–1234 (2015)
25. R. Ma, Y. Wang, B. Cui, Y. Wang, J. Mater. Sci.: Mater. Electron. **28**(15), 10986–10991 (2017)
26. X. Chen, X. Li, G. Huang, G. Liu, X. Yan, J. Mater. Sci.: Mater. Electron. **28**(22), 17278–17282 (2017)
27. Y. Wang, B. Cui, M. Shangguan, S. Wang, J. Mater. Sci.: Mater. Electron. **29**(8), 6369–6376 (2018)
28. R. Guinebretière, *X-Ray Diffraction by Polycrystalline Materials*, 1st edn. (Wiley, London, 2007), pp. 94–97
29. Y. Liu, B. Cui, Y. Wang, J. Am. Ceram. Soc. **99**(5), 1664–1670 (2016)
30. R. Berthelot, B. Basly, S. Buffière, J. Majimel, G. Chevallier, A. Weibel, J. Mater. Chem. C **2**(4), 683–690 (2014)
31. M.H. Frey, Z. Xu, P. Han, D.A. Payne, Ferroelectrics **206**(1), 337–353 (1998)
32. T.A. Vanderah, T. Siegrist, R.S. Roth, A.P. Ramirez, R.G. Geyer, Eur. J. Inorg. Chem. **2004**(12), 2434–2441 (2004)
33. S. Liu, L. Zhang, J. Wang, Y. Zhao, X. Wang, Ceram. Int. **43**(14), 10683–10690 (2017)
34. A. Berenov, F. Le Goupil, N. Alford, Sci. Rep. **6**, 28055 (2016)
35. Y. Sun, H. Liu, H. Hao, S. Zhang, J. Am. Ceram. Soc. **99**(9), 3067–3073 (2016)